Carborane Complexes of Ruthenium: Synthesis and Structural Studies of Di- and Triruthenium Carbonyl Species†

Yi-Hsien Liao, Donald F. Mullica, Eric L. Sappenfield, and F. Gordon A. Stone*

Department of Chemistry, Baylor University, Waco, Texas 76798-7348

Received May 14, 1996[⊗]

The compounds $[Ru_3(CO)_{12}]$ and *nido*-7,8-Me_2-7,8-$C_2B_9H_{11}$ react in CH_2Cl_2 to yield a mixture of $[Ru(CO)_3(\eta^5\text{-}7,8\text{-}Me_2\text{-}7,8\text{-}C_2B_9H_9)]$ (**1b**) and $[Ru_3(CO)_8(\eta^5\text{-}7,8\text{-}Me_2\text{-}7,8\text{-}C_2B_9H_9)]$ (**2**) in a ratio of ca. 1:2. The tri- and dinuclear ruthenium complexes $[Ru_3(\mu\text{-}H)(\mu\text{-}\sigma\text{:}\eta^5\text{-}7,8\text{-}Me_2\text{-}7,8\text{-}C_2B_9H_8)(CO)_7(PR_3)]$ (PR_3 = PPh_3 (**3**), PCy_3 (**6**)), $[Ru_3(\mu\text{-}H)(\mu\text{-}\sigma\text{:}\eta^5\text{-}7,8\text{-}Me_2\text{-}7,8\text{-}C_2B_9H_8)(CO)_6(PR_3)_2]$ (PR_3 = PPh_3 (**4**), PMe_2Ph (**5**)), $[Ru_2(CO)_4(PMe_3)_2(\eta^5\text{-}7,8\text{-}Me_2\text{-}7,8\text{-}C_2B_9H_9)]$ (**7**), and $[Ru_3(\mu\text{-dppm})(CO)_6(\eta^5\text{-}7,8\text{-}Me_2\text{-}7,8\text{-}C_2B_9H_9)]$ (**8**) have been prepared by treating **2** with tertiary phosphines. A single-crystal X-ray diffraction study on **5** revealed the structure as one in which a triangular array of ruthenium atoms is bridged by a *nido*-7,8-Me_2-7,8-$C_2B_9H_8$ group. The latter is pentahapto coordinated to one Ru atom, which carries two CO ligands, and is linked to the other metal atoms by a Ru−B and a B−H⇀Ru bond, respectively. These two ruthenium atoms are each coordinated by two CO groups and one PMe_2Ph group. Treatment of **2** with $Me_2NCH_2NMe_2$ in CH_2Cl_2 affords a mixture of the complexes $[Ru_2(\mu\text{-}\eta^5\text{-}7,8\text{-}Me_2\text{-}10\text{-}CH_2NMe_2\text{-}7,8\text{-}C_2B_9H_8)(CO)_5]$ (**9**) and $[Ru_2(CO)_5(NHMe_2)(\eta^5\text{-}7,8\text{-}Me_2\text{-}7,8\text{-}C_2B_9H_9)]$ (**10**). The structures of both diruthenium compounds were established by X-ray diffraction. In **9** the Ru−Ru bond is bridged by the 7,8-Me_2-10-CH_2NMe_2-7,8-$C_2B_9H_8$ cage system. The open pentagonal CCBBB face is coordinated to one Ru atom, which also carries two CO molecules, while the exopolyhedral CH_2NMe_2 group is coordinated to the other Ru atom which is also ligated by three CO molecules. In **10** a $Ru(CO)_2(\eta^5\text{-}7,8\text{-}Me_2\text{-}7,8\text{-}C_2B_9H_9)$ moiety with a *closo*-3,1,2-RuC_2B_9 framework is linked by exopolyhedral Ru−Ru and B−H⇀Ru bonds to a $Ru(CO)_3(NHMe_2)$ group. The reaction between **2** and pyridine affords a mixture of $[Ru_2(CO)_5(NC_5H_5)(\eta^5\text{-}7,8\text{-}Me_2\text{-}7,8\text{-}C_2B_9H_9)]$ (**11**) and $[Ru_2(CO)_4(NC_5H_5)_2(\eta^5\text{-}7,8\text{-}Me_2\text{-}7,8\text{-}C_2B_9H_9)]$ (**12**). An X-ray diffraction study on **11** revealed a molecular structure similar to that of **10**. The new compounds have been characterized by NMR spectroscopy in addition to the X-ray diffraction studies.

Introduction

We reported recently that the mononuclear ruthenium complex $[Ru(CO)_3(\eta^5\text{-}7,8\text{-}C_2B_9H_{11})]$ (**1a**) (Chart 1) can be readily prepared by heating $[Ru_3(CO)_{12}]$ with *nido*-7,8-$C_2B_9H_{13}$ in heptane at reflux temperatures.[1] No polynuclear ruthenium species were isolated from this reaction. In contrast, as described in this paper, the corresponding reaction between $[Ru_3(CO)_{12}]$ and *nido*-7,8-Me_2-7,8-$C_2B_9H_{11}$ affords a mixture of the mono- and trinuclear ruthenium complexes $[Ru(CO)_3(\eta^5\text{-}7,8\text{-}Me_2\text{-}7,8\text{-}C_2B_9H_9)]$ (**1b**) and $[Ru_3(CO)_8(\eta^5\text{-}7,8\text{-}Me_2\text{-}7,8\text{-}C_2B_9H_9)]$ (**2**), with the latter as the predominant product. The favored formation of the triruthenium species when the carbon vertices in the *nido*-carborane precursor carry methyl substituents rather than hydrogen is intriguing although the reason for this remains unresolved. However, the nature of metallacarborane complexes produced in syntheses is known to be much influenced by the presence or absence of substituents on the carbon vertices of the precursor.[2] Evidently the formation of **2** and the nonformation of $[Ru_3(CO)_8(\eta^5\text{-}7,8\text{-}C_2B_9H_{11})]$ in the previous work[1] is a further manifestation of this behavior.

As far as we are aware, the cluster compound **2** and the compounds $[NEt_4][Mo_3(\mu_3\text{-}CC_6H_4Me\text{-}4)(\mu\text{-}CO)(CO)_8(\eta^5\text{-}7,8\text{-}C_2B_9H_{11})]$[3] and $[Ru_3(CO)_8(\eta^5\text{-}7\text{-}NR_3\text{-}7\text{-}CB_{10}H_{10})]$[4] are the only known homonuclear trimetal species of the transition elements having a carborane ligand attached to the metal triangle, although several heteronuclear trimetal compounds with these ligands have been characterized.[2] Compound **2** has a potentially interesting derivative chemistry, hence in addition to its synthesis we describe herein reactions with several donor molecules.

* To whom correspondence should be addressed.

† In the compounds described in this paper ruthenium atoms and *nido*-C_2B_9 cages form *closo*-1,2-dicarba-3-ruthenadodecaborane structures. However, use of this numbering scheme leads to a complicated nomenclature for the polynuclear metal complexes reported. Following precedent (Mullica, D. F.; Sappenfield, E. L.; Stone, F. G. A.; Woollam, S. F. *Organometallics* **1994**, *13*, 157) therefore we treat the cage as a *nido* 11-vertex ligand with numbering as for an icosahedron from which the twelfth vertex has been removed. This has the added convenience of relating the metallacarborane complexes to isolobal species with η^5-C_5H_5 ligands.

⊗ Abstract published in *Advance ACS Abstracts,* November 1, 1996.

(1) Anderson, S.; Mullica, D. F.; Sappenfield, E. L.; Stone, F. G. A. *Organometallics* **1995**, *14*, 3516.

(2) (a) Stone, F. G. A. *Adv. Organomet. Chem.* **1990**, *31*, 135. (b) Brew, S. A.; Stone, F. G. A. *Adv. Organomet. Chem.* **1993**, *35*, 135. (c) Jelliss, P. A.; Stone, F. G. A. *J. Organomet. Chem.* **1995**, *500*, 307.

(3) Dossett, S. J.; Hart, I. J.; Stone, F. G. A. *J. Chem. Soc., Dalton Trans.* **1990**, 3489.

(4) Lebedev, V. N.; Mullica, D. F.; Sappenfield, E. L.; Stone, F. G. A. *Organometallics* **1996**, *15*, 1669.

S0276-7333(96)00362-7 CCC: $12.00

Table 1. Analytical and Physical Data

compd	color	yield/%	ν_{max}(CO)[a]/cm^{-1}	anal./%[b] C	H
[Ru(CO)$_3$(η^5-7,8-Me$_2$-7,8-C$_2$B$_9$H$_9$)] (**1b**)	pale yellow	20	2110 s, 2054 s	24.4 (24.3)	4.4 (4.4)
[Ru$_3$(CO)$_8$(η^5-7,8-Me$_2$-7,8-C$_2$B$_9$H$_9$)] (**2**)	orange-red	40	2096 s, 2060 s, 2026 s, 2000 m, 1960 w	23.8 (24.1)[c]	2.8 (2.9)
[Ru$_3$(μ-H)(μ-σ:η^5-7,8-Me$_2$-7,8-C$_2$B$_9$H$_8$)(CO)$_7$(PPh$_3$)] (**3**)	red	54	2074 s, 2050 s, 2014 s, 1994 s, 1932 w	38.1 (37.8)	3.5 (3.3)
[Ru$_3$(μ-H)(μ-σ:η^5-7,8-Me$_2$-7,8-C$_2$B$_9$H$_8$)(CO)$_6$(PPh$_3$)$_2$] (**4**)	red	76	2054 s, 2014 s, 1996 w, 1974 m, 1948 m	45.8 (45.5)[d]	3.6 (3.8)
[Ru$_3$(μ-H)(μ-σ:η^5-7,8-Me$_2$-7,8-C$_2$B$_9$H$_8$)(CO)$_6$(PMe$_2$Ph)$_2$] (**5**)	red	74	2048 s, 2010 s, 1988 w, 1968 m, 1944 m	33.8 (34.4)	4.1 (4.1)
[Ru$_3$(μ-H)(μ-σ:η^5-7,8-Me$_2$-7,8-C$_2$B$_9$H$_8$)(CO)$_7$(PCy$_3$)] (**6**)	red	55	2070 m, 2040 s, 2008 sh, 1990 s, 1932 w	38.7 (39.1)[c]	6.0 (5.6)
[Ru$_2$(CO)$_4$(PMe$_3$)$_2$(η^5-7,8-Me$_2$-7,8-C$_2$B$_9$H$_9$)] (**7**)	orange-red	66	1988 s, 1954 s, 1898 m	26.9 (26.8)	5.5 (5.3)
[Ru$_3$(μ-dppm)(CO)$_6$(η^5-7,8-Me$_2$-7,8-C$_2$B$_9$H$_9$)] (**8**)	red	29	2032 s, 1994 s, 1976 sh, 1938 w	45.1 (44.2)[e]	4.4 (4.5)
[Ru$_2$(μ-η^5-7,8-Me$_2$-10-CH$_2$NMe$_2$-7,8-C$_2$B$_9$H$_8$)(CO)$_5$] (**9**)	orange-red	4	2084 s, 2018 s, 1984 m, 1942 m	25.5 (25.8)[f]	3.9 (4.0)
[Ru$_2$(CO)$_5$(NHMe$_2$)(η^5-7,8-Me$_2$-7,8-C$_2$B$_9$H$_9$)] (**10**)	orange-red	22	2096 s, 2028 s, 1976 s, 1928 s	23.6 (24.1)[g]	3.9 (4.1)
[Ru$_2$(CO)$_5$(NC$_5$H$_5$)(η^5-7,8-Me$_2$-7,8-C$_2$B$_9$H$_9$)] (**11**)	orange-red	8	2094 s, 2030 s, 1972 m, 1926 m	28.0 (28.9)[h]	3.4 (3.5)
[Ru$_2$(CO)$_4$(NC$_5$H$_5$)$_2$(η^5-7,8-Me$_2$-7,8-C$_2$B$_9$H$_9$)] (**12**)	orange-red	26	2038 s, 1976 s, 1970 sh, 1906 s	32.5 (31.8)[d,i]	3.7 (3.8)

[a] Measured in CH_2Cl_2. A medium-intensity broad band observed at ca. 2550 cm^{-1} in the spectra of all the compounds is due to B−H absorptions. [b] Calculated values are given in parentheses. [c] Crystallizes with 0.5 molecule of *n*-pentane. [d] Crystallizes with 1 molecule of CH_2Cl_2. [e] Crystallizes with 1 molecule of *n*-pentane. [f] N 2.4 (2.5). [g] N 2.4 (2.6). [h] N 2.4 (2.4). [i] N 4.2 (3.9).

Chart 1

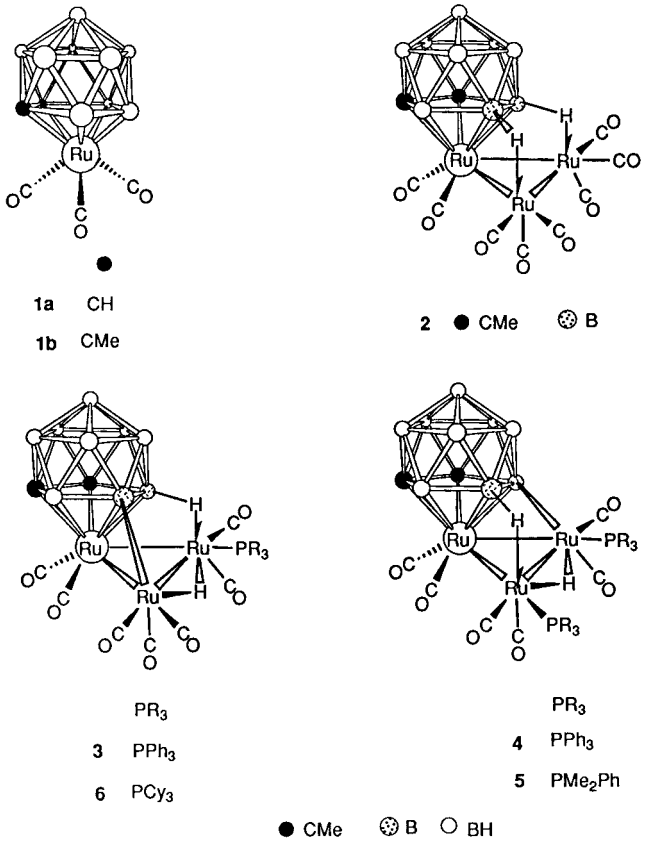

Results and Discussion

The mono- and trinuclear ruthenium complexes **1b** and **2** are readily formed in a ratio of ca. 1:2 by heating [Ru$_3$(CO)$_{12}$] with *nido*-7,8-Me$_2$-7,8-C$_2$B$_9$H$_{11}$ in CH_2Cl_2. The compounds are separable by column chromatography on silica gel and were characterized by the data listed in Tables 1−3. The microanalytical and spectroscopic data for **1b** are in accord with its formulation as an analog of **1a** with the cage carbons carrying Me substituents. For **2** the ^{1}H, ^{11}B{^{1}H}, and ^{11}B NMR data are in agreement with it being a triruthenium complex. One ruthenium center is pentahapto coordinated by the *nido*-7,8-Me$_2$-7,8-C$_2$B$_9$H$_9$ fragment which forms two exopolyhedral B−H→Ru bonds to the other two ruthenium atoms. The structure is asymmetric since one B−H→Ru linkage employs a boron atom adjacent to carbon in the open CC*B*BB ring ligating the Ru atom, and the other employs the unique boron atom in the CCB*B*B ring which has no connectivity with the carbons. In accord with this asymmetry, the nonequivalent CMe groups give rise to two signals (δ 2.22 and 2.47) in the ^{1}H NMR spectrum and four resonances (δ 62.5, 74.3 (*C*Me); δ 30.2, 32.5 (C*Me*)) in the ^{13}C{^{1}H} spectrum (Table 2).

In the ^{1}H NMR spectrum the nonequivalent B−H→Ru groups give rise to only one quartet (δ −10.23) in the chemical shift range diagnostic for a B−H→Ru three-center two-electron bond.[2b] This quartet is very broad, however, and since its relative intensity corresponds to two protons it must result from overlapping of two sets of peaks. In contrast, the ^{11}B{^{1}H} spectrum shows two resonances (δ 15.8 and 24.4) attributable to the nonequivalent B−H→Ru groups (Table 3). Diagnostically for these groups, in the fully coupled ^{11}B NMR spectrum these signals became doublets with ^{1}H−^{11}B couplings of 76 and 62 Hz, respectively, as compared with values of ca. 120−140 Hz observed for the doublet resonances for the terminal B−H groups.[2b] The ^{13}C{^{1}H} NMR spectrum of **2** shows seven resonances for the eight CO groups, but one peak has an intensity corresponding to two carbonyl ligands (Table 2). This pattern is in agreement with the overall asymmetry. The mode of bonding of the *nido*-7,8-Me$_2$-7,8-C$_2$B$_9$H$_9$ group to the metal triangle in **2** with pentahapto coordination to one metal atom producing a *closo*-3,1,2-RuC$_2$B$_9$ framework and concomitant formation of two exopolyhedral B−H→Ru bonds to the other metal centers is very common and has been established by X-ray diffraction in several heteronuclear trimetal complexes.[2] Moreover, the monocarbon-carborane triruthenium zwitterionic complex [Ru$_3$(CO)$_8$(η^5-7-NMe$_3$-7-CB$_{10}$H$_{10}$)] similarly has two B−H→Ru bridge bonds.[4]

Reactions of **2** with various donor ligands were investigated. Treatment of **2** with PPh$_3$ in THF at room temperature gave [Ru$_3$(μ-H)(μ-σ:η^5-7,8-Me$_2$-7,8-C$_2$B$_9$H$_8$)(CO)$_7$(PPh$_3$)] (**3**), whereas when the reaction was carried out in the same solvent at reflux temperature the bis(phosphine) complex [Ru$_3$(μ-H)(μ-σ:η^5-7,8-Me$_2$-7,8-C$_2$B$_9$H$_8$)(CO)$_6$(PPh$_3$)$_2$] (**4**) was formed. A similar bis(phosphine) complex [Ru$_3$(μ-H)(μ-σ:η^5-7,8-Me$_2$-7,8-C$_2$B$_9$H$_8$)(CO)$_6$(PMe$_2$Ph)$_2$] (**5**) was obtained by treating **2** with excess of PMe$_2$Ph in CH_2Cl_2 at room temperature. Data characterizing complexes **3**−**5** are given in Tables 1−3. All three molecules have a similar framework structure which was established for **5** by an X-ray diffraction

Table 2. Hydrogen-1 and Carbon-13 NMR Data[a]

compd	$\delta(^1H)$[b]	$\delta(^{13}C)$[c]
1b	2.30 (s, 6H, Me)	189.6 (CO), 78.7 (*C*Me), 32.9 (C*Me*)
2	−10.23 (q vbr, 2 H, B−H→Ru), 2.22, 2.47 (s × 2, 6 H, CMe)	200.1, 199.8, 198.3, 195.5, 190.2, 189.8 (CO), 185.4 (CO × 2), 74.3, 62.5 (*C*Me), 32.5, 30.2 (C*Me*)
3	−17.51 (s br, 1 H, Ru(*μ*-H)Ru), −9.30 (m vbr, 1 H, B−H→Ru), 2.36, 2.48 (s × 2, 6 H, CMe), 7.40−7.60 (m, 15 H, Ph)	201.7, 198.8, 198.5, 196.2, 195.2, 194.0, 192.1 (CO), 134.1−128.8 (Ph), 73.2, 62.1 (*C*Me), 33.3, 32.5 (C*Me*)
4	−16.22 (s br, 1 H, Ru(*μ*-H)Ru), −9.40 (m vbr, 1 H, B−H→Ru), 2.35, 2.51 (s × 2, 6 H, CMe), 7.00−7.40 (m, 30 H, Ph)	203.5, 202.1, 201.9, 200.2 (CO), 199.9 (CO × 2), 136.1−128.1 (Ph), 65.9, 62.8 (*C*Me), 33.3, 32.7 (C*Me*)
5	−16.99 (s br, 1 H, Ru(*μ*-H)Ru), −10.08 (q br, 1 H, B−H→Ru, *J*(BH) = 70), 1.57 (d, 3 H, MeP, *J*(PH) = 10), 1.88 (d, 6 H, MeP, *J*(PH) = 10), 1.94 (d, 3 H, MeP, *J*(PH) = 10), 2.39, 2.49 (s × 2, 6 H, CMe), 7.20−7.70 (m, 10 H, Ph)	203.6, 201.3 (CO), 200.4 (CO × 2), 198.1, 193.1 (CO), 142.1−128.1 (Ph), 74.1, 62.6 (*C*Me), 33.6, 32.7 (C*Me*), 22.6 (d, MeP × 2, *J*(PC) = 34), 22.5, 22.1 (d × 2, MeP, *J*(PC) = 34, 35)
6	−18.37 (s br, 1 H, Ru(*μ*-H)Ru), −10.10 (q br, 1 H, B−H→Ru, *J*(BH) = 73), 1.29−1.88 (m, 33 H, C_6H_{11}), 2.38, 2.49 (s × 2, 6 H, CMe)	202.0, 201.4, 200.2, 199.6, 198.9, 197.2, 195.4 (CO), 73.2, 61.7 (*C*Me), 39.1 (d, C_6H_{11}, *J*(PC) = 22), 33.4, 32.6 (C*Me*), 29.7 (d, C_6H_{11}, *J*(PC) = 24), 27.6 (d, C_6H_{11}, *J*(PC) = 11), 26.2 (C_6H_{11})
7	−11.02 (d of q, 1 H, B−H→Ru, *J*(BH) = 78, *J*(PH) = 31), 1.67, 1.73 (d × 2, 18 H, MeP, *J*(PH) = 10, 10), 2.37 (s, 6 H, CMe)	206.2 (CO × 2), 204.3 (d of d, CO × 2, *J*(PC) = 16, 9), 63.2 (*C*Me), 32.0 (C*Me*), 23.0 (d, MeP, *J*(PC) = 34)
8	−9.11 (q br, 2 H, B−H→Ru, *J*(BH) = 80), 2.17, 2.47 (s × 2, 6 H, CMe), 4.62, 4.86 (d of d of d × 2, 2 H, CH_2, *J*(HH) = 14, *J*(PH) = 11, 11), 7.10−7.50 (m, 20 H, Ph)	200.8, 198.4 (CO), 196.4, 192.4 (CO × 2), 138.9−128.5 (Ph), 73.2, 60.0 (*C*Me), 58.8 (d of d, CH_2, *J*(PC) = 26), 32.8, 29.8 (C*Me*)
9	−6.91 (q br, 1 H, B−H→Ru, *J*(BH) = 77), 2.22, 2.30 (s × 2, 6 H, CMe), 2.31, 2.42 (s br × 2, 2 H, BCH_2N), 2.73, 2.83 (s × 2, 6 H, Me_2N)	204.0 (br, CO × 3), 200.5, 197.8 (CO), 66.9 (vbr, *C*Me), 65.2 (CH_2N), 63.6, 62.9 (Me_2N), 33.0, 30.2 (C*Me*)
10	−8.19 (q br, 1 H, B−H→Ru, *J*(BH) = 76), 2.35, 2.37 (s × 2, 6 H, CMe), 2.43, 2.78 (d × 2, 6 H, Me_2N, *J*(HH) = 6), 3.68 (s br, 1 H, NH)	200.7, 200.2 (CO), 65.1 (vbr, *C*Me), 50.2, 48.7 (Me_2N), 31.9, 31.8 (C*Me*)
11	−7.82 (q br, 1 H, B−H→Ru, *J*(BH) = 80), 2.13, 2.33 (s × 2, 6 H, CMe), 7.30−8.30 (m, 5 H, py)	201.7, 200.6 (CO), 154.9, 138.9, 126.3 (py), 65.2, 64.7 (*C*Me), 31.8 (br, C*Me*)
12	−5.28 (q br, 1 H, B−H→Ru, *J*(BH) = 67), 2.15, 2.35 (s × 2, 6 H, CMe), 7.20−8.50 (m, 10 H, py)	203.6, 202.5, 201.1, 200.5 (CO), 155.0−125.8 (py), 63.9 (br, *C*Me), 31.8 (br, C*Me*)

[a] Chemical shifts (δ) in ppm, coupling constants (*J*) in Hz, measurements at ambient temperatures in CD_2Cl_2. [b] Resonances for terminal BH protons occur as broad unresolved signals in the range δ ca. −2 to 3. [c] Hydrogen-1 decoupled; chemical shifts are positive to high frequency of $SiMe_4$.

Table 3. Boron-11 and Phosphorus-31 NMR Data[a]

compd	$\delta(^{11}B)$[b,c]	$\delta(^{31}P)$[d]
1b	9.1 (1 B), −3.6 (2 B), −4.9 (3 B), −8.0 (1 B), −11.1 (2 B)	
2	24.4 (1 B, B−H→Ru, *J*(HB) = 62), 15.8 (1 B, B−H→Ru, *J*(HB) = 76), −3.4 (1 B), −5.1 (3 B), −8.6 (2 B), −10.9 (1 B)	
3	43.0 (1 B, Ru−B), 32.1 (1 B, B−H→Ru, *J*(HB) = 72), −4.6 (3 B), −5.5 (1 B), −7.4 (1 B), −9.3 (2 B)	42.0 (s)
4	44.5 (vbr, 1 B, Ru−B), 32.4 (1 B, B−H→Ru, *J*(HB) = 57), −5.0 (4 B), −9.3 (3 B)	43.3 (s), 53.9 (br s)
5	42.1 (1 B, Ru−B), 32.3 (1 B, B−H→Ru, *J*(HB) = 70), −5.7 (2 B), −6.5 (2 B), −9.5 (3 B)	9.2 (s), 18.2 (s)
6	43.1 (1 B, Ru−B), 32.4 (1 B, B−H→Ru, *J*(HB) = 73), −4.8 (3 B), −7.7 (1 B), −9.8 (2 B), −13.1 (1 B)	67.6 (s)
7	18.3 (1 B, B−H→Ru, *J*(HB) = 78), −8.5 (2 B), −9.9 (2 B), −11.7 (3 B), −18.0 (1 B)	−11.4 (s), −0.1 (s)
8	23.0 (1 B, B−H→Ru, *J*(HB) = 80), 15.6 (1 B, B−H→Ru, *J*(HB) = 70), −5.0 (2 B), −6.5 (2 B), −10.2 (2 B), −12.4 (1 B)	24.7, 21.1 (d × 2, *J*(PP) = 25)
9	24.9 (1 B B−H→Ru, *J*(HB) = 77), −1.6 (1 B), −4.3 (1 B), −5.6 (3 B), −8.2 (1 B), −16.6 (1 B), −19.7 (1 B)	
10	26.6 (1 B, B−H→Ru, *J*(HB) = 76), −6.5 (1 B), −7.5 (1 B), −9.3 (1 B), −10.1 (1 B), −11.1 (2 B), −12.2 (1 B), −17.4 (1 B)	
11	27.7 (1 B, B−H→Ru, *J*(HB) = 80), −6.8 (1 B), −7.7 (1 B), −9.7 (2 B), −11.3 (3 B), −17.7 (1 B)	
12	20.4 (1 B, B−H→Ru, *J*(HB) = 67), −9.1 (2 B), −11.4 (5 B), −17.4 (1 B)	

[a] Measurements at ambient temperatures in CD_2Cl_2. [b] Hydrogen-1 decoupled; chemical shifts (δ) in ppm are positive to high frequency of $BF_3{\cdot}Et_2O$ (external). Signals ascribed to more than one boron nucleus may result from overlapping peaks and do not necessarily indicate symmetry equivalence. [c] The $^1H-^{11}B$ coupling constants (Hz) were measured from fully coupled ^{11}B spectra. [d] Hydrogen-1 decoupled; chemical shifts (δ) in ppm are positive to high frequency of H_3PO_4 (external).

study. The molecule is shown in Figure 1, and selected bond distances and angles are listed in Table 4.

The Ru atoms form a triangular array [Ru(1)−Ru(2) = 2.750(1), Ru(1)−Ru(3) = 2.812(1), Ru(2)−Ru(3) = 2.972(1) Å], with Ru(1) ligated by the *nido*-7,8-C_2B_9 cage in the usual pentahapto mode. The cage bridges the metal triangle via a boron−ruthenium σ-bond and an agostic B−H→Ru interaction. The exopolyhedral B−Ru σ-bond distance [B(5)−Ru(3) = 2.15(1) Å] is the same as that found in [Ru_3(*μ*-H)(*μ*-σ:η^5-7-NMe_3-7-$CB_{10}H_9$)-$(CO)_7(PPh_3)$] which has a very similar structure.[4] The B−H→Ru bond in **5** involves the B(4)H(4) group and Ru(2). Although H(4) was not directly located from the difference Fourier mapping, its presence was clearly revealed by the NMR data, discussed below. The separations B(4)−Ru(2) [2.34(1) Å], B(4)−H(4) (ca. 1.12 Å), and Ru(2)−H(4) (ca. 1.77 Å) compare well with the corresponding parameters for the B−H→Ru group in [Ru_3(*μ*-H)(*μ*-σ:η^5-7-NMe_3-7-$CB_{10}H_9$)$(CO)_7(PPh_3)$] of 2.37(1), 1.08, and 1.76 Å, respectively.

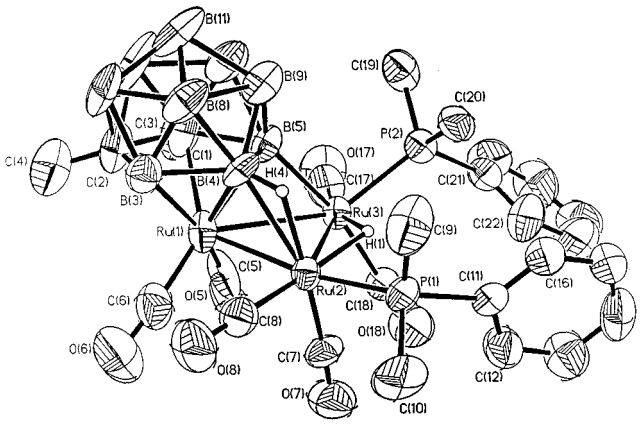

Figure 1. Molecular structure of [Ru_3(*μ*-H)(*μ*-σ:η^5-7,8-Me_2-7,8-$C_2B_9H_8$)$(CO)_6(PMe_2Ph)_2$] (**5**), showing the crystallographic labeling scheme. Except for H(1) and H(4), hydrogen atoms have been omitted for clarity, and thermal ellipsoids are shown at 50% probability level.

Table 4. Selected Internuclear Distances (Å) and Angles (deg) for [$Ru_3(\mu\text{-}\sigma\text{:}\eta^5$-7,8-$Me_2$-7,8-$C_2B_9H_8$)$(CO)_6(PMe_2Ph)_2$] (5), with Estimated Standard Deviations in Parentheses

Ru(1)−C(1)	2.26(1)	Ru(1)−C(2)	2.31(1)	Ru(1)−B(3)	2.24(2)	Ru(1)−B(4)	2.22(1)
Ru(1)−B(5)	2.22(1)	Ru(1)−C(5)	1.88(1)	Ru(1)−C(6)	1.82(1)	Ru(1)−Ru(2)	2.750(1)
Ru(1)−Ru(3)	2.812(1)	H(1)−Ru(2)	1.78	H(1)−Ru(3)	1.78	C(1)−C(2)	1.65(2)
C(1)−B(5)	1.82(2)	C(1)−B(6)	1.75(3)	C(1)−B(10)	1.76(2)	C(1)−C(3)	1.57(2)
C(2)−B(3)	1.71(2)	C(2)−B(6)	1.75(3)	C(2)−B(7)	1.70(2)	C(2)−C(4)	1.46(2)
B(3)−B(4)	1.76(2)	B(3)−B(7)	1.76(2)	B(3)−B(8)	1.77(2)	B(4)−H(4)	1.12
B(4)−B(5)	1.82(2)	B(4)−B(8)	1.76(2)	B(4)−B(9)	1.79(2)	B(4)−Ru(2)	2.34(1)
H(4)−Ru(2)	1.77	B(5)−B(9)	1.76(2)	B(5)−B(10)	1.83(2)	B(5)−Ru(3)	2.15(1)
B(6)−B(7)	1.73(3)	B(6)−B(10)	1.76(3)	B(6)−B(11)	1.73(3)	B(7)−B(*)	1.80(2)
B(7)−B(11)	1.82(2)	B(8)−B(9)	1.82(2)	B(8)−B(11)	1.83(2)	B(9)−B(10)	1.77(2)
B(9)−B(11)	1.80(3)	B(10)−B(11)	1.77(3)	C(5)−O(5)	1.20(2)	C(6)−O(6)	1.19(2)
Ru(2)−Ru(3)	2.972(1)	Ru(2)−C(7)	1.83(1)	Ru(2)−C(8)	1.87(1)	Ru(2)−P(1)	2.331(3)
C(7)−O(7)	1.17(1)	C(8)−O(8)	1.17(2)	P(1)−C(9)	1.82(1)	P(1)−C(10)	1.79(1)
P(1)−C(11)	1.81(1)	Ru(3)−C(17)	1.82(1)	Ru(3)−C(18)	1.90(1)	Ru(3)−P(2)	2.285(3)
C(17)−O(17)	1.17(2)	C(18)−O(18)	1.17(2)	P(2)−C(19)	1.79(1)	P(2)−C(20)	1.77(1)
P(2)−C(21)	1.79(1)						
C(5)−Ru(1)−C(6)	83.6(6)	C(5)−Ru(1)−Ru(2)	106.1(4)	C(5)−Ru(1)−Ru(3)	69.4(4)	C(6)−Ru(1)−Ru(2)	88.1(5)
C(6)−Ru(1)−Ru(3)	132.5(5)	B(4)−Ru(1)−Ru(2)	54.8(3)	B(5)−Ru(1)−Ru(3)	48.8(4)	Ru(2)−Ru(1)−Ru(3)	64.6(1)
Ru(2)−H(1)−Ru(3)	113.2(1)	Ru(1)−B(4)−H(4)	120.8(9)	B(4)−H(4)−Ru(2)	105.7(7)	Ru(1)−B(5)−Ru(3)	80.2(5)
Ru(1)−C(5)−O(5)	174.2 (12)	Ru(1)−C(6)−O(6)	176.3(14)	C(7)−Ru(2)−C(8)	92.0(5)	Ru(1)−Ru(2)−H(1)	90.4(1)
Ru(1)−Ru(2)−H(4)	78.5(1)	H(1)−Ru(2)−H(4)	85.5(1)	Ru(1)−Ru(2)−C(7)	94.7(4)	H(1)−Ru(2)−C(7)	92.4(4)
H(4)−Ru(2)−C(7)	172.8(4)	Ru(1)−Ru(2)−C(8)	92.8(4)	H(1)−Ru(2)−C(8)	174.3(4)	H(4)−Ru(2)−C(8)	90.6(4)
Ru(1)−Ru(2)−P(1)	171.4(1)	H(1)−Ru(2)−P(1)	85.3(1)	H(4)−Ru(2)−P(1)	93.7(1)	C(7)−Ru(2)−P(1)	92.9(4)
C(8)−Ru(2)−P(1)	90.9(4)	Ru(1)−Ru(2)−Ru(3)	58.7(1)	H(1)−Ru(2)−Ru(3)	33.4(1)	H(4)−Ru(2)−Ru(3)	89.6(1)
C(7)−Ru(2)−Ru(3)	84.9(4)	C(8)−Ru(2)−Ru(3)	150.8(4)	P(1)−Ru(2)−Ru(3)	118.1(1)	Ru(2)−C(7)−O(7)	177.4(11)
Ru(2)−C(8)−O(8)	178.5(11)	Ru(2)−P(1)−C(9)	112.7(5)	Ru(2)−P(1)−C(10)	114.7(5)	Ru(2)−P(1)−C(11)	118.5(4)
Ru(1)−Ru(3)−Ru(2)	56.7(1)	Ru(1)−Ru(3)−H(1)	88.3(1)	Ru(1)−Ru(3)−B(5)	51.0(4)	Ru(1)−Ru(3)−C(17)	104.7(4)
Ru(1)−Ru(3)−C(18)	116.5(4)	Ru(1)−Ru(3)−P(2)	143.5(1)	Ru(2)−Ru(3)−B(5)	76.1(4)	Ru(2)−Ru(3)−C(17)	160.8(4)
Ru(2)−Ru(3)−C(18)	94.0(4)	Ru(2)−Ru(3)−P(2)	113.6(1)	C(17)−Ru(3)−C(18)	90.4(6)	H(1)−Ru(3)−B(5)	87.5(4)
H(1)−Ru(3)−C(17)	165.8(4)	H(1)−Ru(3)−C(18)	88.7(4)	H(1)−Ru(3)−P(2)	81.9(1)	B(5)−Ru(3)−C(17)	96.3(6)
B(5)−Ru(3)−C(18)	167.0(5)	B(5)−Ru(3)−P(2)	93.3(4)	C(17)−Ru(3)−P(2)	84.1(4)	C(18)−Ru(3)−P(2)	98.5(4)
Ru(3)−C(17)−O(17)	176.7(11)	Ru(3)−C(18)−O(18)	179.1(10)	Ru(3)−P(2)−C(19)	115.5(5)	Ru(3)−P(2)−C(20)	116.0(4)
Ru(3)−P(2)−C(21)	113.4(4)						

	distances (Ph)		angles (Ph)	
ring	mean	range	mean	range
C(11)−C(16)	1.38(1)	1.363−1.394	120(2)	116.7−112.5
C(21)−C(26)	1.38(1)	1.363−1.391	120(4)	115.0−126.1

An important feature of the structure of **5** is the presence of the hydrido ligand H(1) bridging Ru(2)−Ru(3) which, as expected, is the longest of the three metal−metal distances. The location of H(1) was based on potential-energy minimization calculations,[5] but the μ-H−Ru distances (1.78 Å) are in the normal range[6] and compare with 1.72 Å for the hydrido bridge in [$Ru_3(\mu$-H)$(\mu\text{-}\sigma\text{:}\eta^5$-7-$NMe_3$-7-$CB_{10}H_9$)$(CO)_7(PPh_3)$].[4] Each Ru atom in **5** carries two terminally bound CO groups, but Ru(2) and Ru(3) are also ligated by PMe_2Ph molecules. The distances Ru(2)−P(1) [2.331(3) Å] and Ru(3)−P(2) [2.285(3) Å] are in excellent agreement with the data for such bonds in related structures.[7] Atom P(1) is transoid to Ru(1) [Ru(1)−Ru(2)−P(1) = 171.4(1)°] while P(2) is cisoid to B(5) [P(2)−Ru(3)−B(5) = 93.3(4)°].

The NMR data for **5** (Tables 2 and 3) are in agreement with the results of the X-ray diffraction study, and the data for **3** and **4** with similar structures are also in accord with the formulations for these species. The ^{1}H NMR spectrum of **5** shows diagnostic resonances for the Ru(μ-H)Ru[8] and B−H⇀Ru[1,2b] groups at δ −16.99 and −10.08, respectively, with the latter signal seen as a quartet [J(BH) = 70 Hz] as expected. In the fully coupled ^{11}B NMR spectrum there is a diagnostic singlet peak at δ 42.1 for the B−Ru group and doublet resonances for the other signals. However, the resonance at δ 32.3 is in the chemical shift region for a B−H⇀Ru system, and in accord with this assignment the ^{1}H−^{11}B coupling was 70 Hz. The asymmetry in **5** would lead to nonequivalence of the cage CMe groups. Thus as expected there are two signals (δ 2.39 and 2.49) for these groups in the ^{1}H NMR spectrum and four (δ 62.6, 74.1 (*C*Me); δ 32.7, 33.6 (C*Me*)) in the ^{13}C{^{1}H} NMR spectrum. Although five rather than six CO resonances are observed in the latter spectrum, one signal corresponded in intensity to an overlap of two peaks (Table 2).

The ^{1}H NMR data for the monosubstituted phosphine complex **3** revealed signals for the Ru(μ-H)Ru and B−H⇀Ru groups at δ −17.51 and −9.30, respectively, and for the cage CMe groups at δ 2.36 and 2.48. The ^{13}C{^{1}H} NMR spectrum displayed seven peaks for the nonequivalent CO ligands, and there were the expected resonances for the cage CMe groups at δ 62.1 and 73.2 (*C*Me) and at δ 32.5 and 33.3 (C*Me*). In a fully coupled ^{11}B NMR spectrum a singlet at δ 43.0 could be assigned to the B−Ru group and a doublet [J(HB) = 72 Hz] at δ 32.1 to the B−H⇀Ru moiety. The ^{31}P{^{1}H} NMR spectrum showed a singlet at δ 42.0. Complex **3** is assigned a structure in which the PPh_3 group is attached to the Ru atom involved in the B−H⇀Ru bridge system. The three-center two-electron bond corresponds to an incipient oxidative addition at the metal center. The structural assignment is made by analogy with a recent X-ray diffraction study of [$Ru_3(\mu$-H)$(\mu\text{-}\sigma\text{:}\eta^5$-7-$NMe_3$-7-$CB_{10}H_9$)$(CO)_7(PPh_3)$] which established that the phosphine group in this molecule is similarly placed on

(5) Orpen, A. G. *J. Chem. Soc., Dalton Trans.* **1980**, 2509.
(6) Teller, R. G.; Bau, R. *Struct. Bonding* **1981**, *44*, 1.
(7) Orpen, A. G.; Brammer, L.; Allen, F. H.; Kennard, O.; Watson, D. G.; Taylor, R. *J. Chem. Soc., Dalton Trans.* **1989**, S1.
(8) Kaesz, H. D.; Saillant, R. B. *Chem. Rev.* **1972**, *72*, 231.

Chart 2

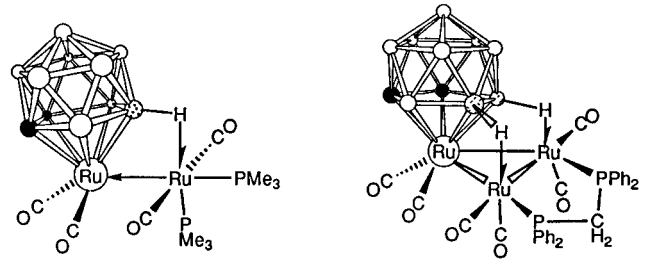

an Ru atom involved in a B−H→Ru bridge.[4] An alternative structure for **3** with the PPh_3 group linked to the ruthenium atom which forms the Ru−B σ-bond might be thought more likely because substitution of a CO molecule by the superior donor PPh_3 would increase the nucleophilicity of the ruthenium center to which it is attached. This would promote oxidative addition at that center so as to yield the B−Ru and Ru(μ-H)Ru units. However, as discussed previously,[4] a structure with the PPh_3 ligand attached to the ruthenium which is also σ-bonded to a cage boron might be kinetically unstable and undergo rearrangement of its B−Ru and B−H→Ru groups between adjacent boron atoms in the CCBBB ring. This could be facilitated by migration of hydrogen from the Ru(μ-H)Ru bridge to a B−H→Ru site.

The tricyclohexylphosphine complex $[Ru_3(\mu\text{-H})(\mu\text{-}\sigma\text{:}\eta^5\text{-}7,8\text{-}Me_2\text{-}7,8\text{-}C_2B_9H_8)(CO)_7(PCy_3)]$ (**6**) was prepared by treating **2** with 1 mol equiv of PCy_3 in CH_2Cl_2 at room temperature. The NMR data (Tables 2 and 3) for **6** are in accord with a formulation akin to **3**. Resonances in the ^{1}H NMR spectrum due to the Ru(μ-H)Ru and B−H→Ru groups are clearly seen at δ −18.37 and −10.10, respectively. In a fully coupled ^{11}B NMR spectrum peaks for the B−Ru and B−H→Ru groups occur as a singlet and a doublet [J(HB) = 73 Hz], respectively, at δ 43.1 and 32.4. The NMR data for **3** (Tables 1 and 2) are very similar.

In contrast, with the reactions with PPh_3, PMe_2Ph, and PCy_3, that between **2** and PMe_3 afforded $[Ru_2(CO)_4(PMe_3)_2(\eta^5\text{-}7,8\text{-}Me_2\text{-}7,8\text{-}C_2B_9H_9)]$ (**7**) (Chart 2), a di- rather than a triruthenium complex. This product was characterized by microanalytical and NMR data (Tables 1−3). In the ^{1}H NMR spectrum there is a diagnostic signal for the B−H→Ru group at δ −11.02, appearing as a doublet of quartets [J(BH) = 78, J(PH) = 31 Hz]. The ^{31}P−^{1}H coupling may be attributed to the PMe_3 group which is transoid to the B−H→Ru bridge. The latter is revealed in the fully coupled ^{11}B NMR spectrum by a doublet resonance at δ 18.3 [J(HB) = 78 Hz]. There are two resonances (δ −11.4 and −0.1) for the non-equivalent PMe_3 ligands in the ^{31}P{^{1}H} NMR spectrum. In a dimetal complex with a B−H→Ru bridging unit it is usual for the latter to involve the B atom in the β site with respect to the carbons in the open CCB*B*B face coordinated to the Ru.[2] For **7** this configuration would lead to a plane of symmetry through the Ru and P atoms, the B atom in the β site, and the midpoint of the cage C−C connectivity. This symmetrical structure is supported by the ^{1}H NMR spectrum which displays only one resonance (δ 2.37) for the cage CMe protons. Correspondingly, in the ^{13}C{^{1}H} NMR spectrum the equivalence of the cage CMe fragments results in only two signals (δ 63.2 (*C*Me) and 32.0 (C*Me*)) for these groups. The observed pattern of only two peaks for the CO resonances is also in agreement with the symmetry. The resonance at δ 206.2 can be assigned to the carbonyl-carbon nuclei in the cisoid $Ru(CO)_2$ group coordinated by the open face of the *nido*-C_2B_9 cage, the two carbonyls lying on either side of the symmetry plane, while the doublet-of-doublets at δ 204.3 is attributable to the equivalent carbonyls of the transoid $Ru(CO)_2$ fragment, with ^{31}P−^{13}C coupling to the non-equivalent PMe_3 groups.

Reaction of **2** with $Ph_2PCH_2PPh_2$ (dppm) afforded $[Ru_3(\mu\text{-dppm})(CO)_6(\eta^5\text{-}7,8\text{-}Me_2\text{-}7,8\text{-}C_2B_9H_9)]$ (**8**) characterized by the data given in Tables 1−3. NMR spectroscopy indicated that the molecular structure is similar to that of **2**, with the dppm ligand bridging the Ru−Ru bond formed by the two metal atoms not pentahapto coordinated by the cage. The absence of B−Ru and Ru(μ-H)Ru groups in the molecule, akin to those present in **3**−**5**, may be due to the μ-dppm group occupying the bridging site thus impeding the fully oxidative step from a B−H→Ru linkage into B−Ru and Ru(μ-H)Ru. The two B−H→Ru groups in **8** are non-equivalent since one employs a BH group β to the carbons in the C_2B_3 ring while the other uses a BH bond α to the ring carbons. Nevertheless, in the ^{1}H NMR spectrum only one very broad quartet signal is seen at δ −9.11. However, its relative intensity indicated that it was due to two protons. Evidently the resonances for the two B−H→Ru groups are essentially coincident in the ^{1}H NMR spectrum as was observed for **2**. However, two doublet resonances for the B−H→Ru groups were seen at δ 23.0 and 15.6 in a fully coupled ^{11}B NMR spectrum, with ^{1}H−^{11}B couplings of ca. 70−80 Hz. As expected due to the asymmetry, there are two resonances in the ^{31}P{^{1}H} NMR spectrum (Table 3), each a doublet [J(PP) = 25 Hz]. The nonequivalence of the CMe cage vertices is indicated in the ^{1}H NMR spectrum by the appearance of peaks at δ 2.17 and 2.47 and in the ^{13}C{^{1}H} NMR spectrum by resonances at δ 60.0 and 73.2 (*C*Me) and δ 29.8 and 32.8 (C*Me*). The nonequivalent PCH_2P hydrogens were revealed in the ^{1}H NMR spectrum by doublets-of-doublets-of-doublets at δ 4.62 and 4.86 [J(HH) = 14; J(PH) = 11 and 11 Hz].

Reactions between compound **2** and some nitrogen bases were next investigated. Reaction with $Me_2NCH_2NMe_2$ afforded a mixture of the two diruthenium species $[Ru_2(\mu\text{-}\eta^5\text{-}7,8\text{-}Me_2\text{-}10\text{-}CH_2NMe_2\text{-}7,8\text{-}C_2B_9H_8)(CO)_5]$ (**9**) and $[Ru_2(CO)_5(NHMe_2)(\eta^5\text{-}7,8\text{-}Me_2\text{-}7,8\text{-}C_2B_9H_9)]$ (**10**). Evidently the reaction is complex proceeding with fission

Table 5. Selected Internuclear Distances (Å) and Angles (deg) for [$Ru_2(\mu\text{-}\eta^5\text{-}7,8\text{-}Me_2\text{-}10\text{-}CH_2NMe_2\text{-}7,8\text{-}C_2B_9H_8)(CO)_5$] (9), with Estimated Standard Deviations in Parentheses

Ru(1)−C(1)	2.244(4)	Ru(1)−C(2)	2.242(5)	Ru(1)−B(3)	2.199(6)	Ru(1)−B(4)	2.274(4)
Ru(1)−B(5)	2.240(5)	Ru(1)−C(8)	1.857(5)	Ru(1)−C(9)	1.887(4)	Ru(1)−Ru(2)	2.727(1)
C(1)−C(2)	1.700(8)	C(1)−B(5)	1.738(7)	C(1)−B(6)	1.737(8)	C(1)−B(10)	1.707(6)
C(1)−C(3)	1.523(6)	C(2)−B(3)	1.735(6)	C(2)−B(6)	1.720(7)	C(2)−B(7)	1.707(7)
C(2)−C(4)	1.521(6)	B(3)−H(3)	1.104	B(3)−B(4)	1.775(9)	B(3)−B(7)	1.777(7)
B(3)−B(8)	1.771(6)	B(3)−Ru(2)	2.410(5)	H(3)−Ru(2)	1.796	B(4)−B(5)	1.834(8)
B(4)−B(8)	1.787(8)	B(4)−B(9)	1.793(7)	B(4)−C(5)	1.599(6)	B(5)−B(9)	1.796(7)
B(5)−B(10)	1.782(7)	B(6)−B(7)	1.727(9)	B(6)−B(10)	1.768(10)	B(6)−B(11)	1.749(7)
B(7)−B(8)	1.748(7)	B(7)−B(11)	1.756(8)	B(8)−B(9)	1.776(9)	B(8)−B(11)	1.748(7)
B(9)−B(10)	1.782(7)	B(9)−B(11)	1.774(9)	B(10)−B(11)	1.784(9)	C(5)−N(1)	1.527(6)
N(1)−C(6)	1.485(6)	N(1)−C(7)	1.522(7)	N(1)−Ru(2)	2.233(3)	C(8)−O(8)	1.150(7)
C(9)−O(9)	1.163(6)	Ru(2)−C(10)	1.865(5)	Ru(2)−C(11)	1.866(5)	Ru(2)−C(12)	1.923(6)
C(10)−O(10)	1.157(6)	C(11)−O(11)	1.153(6)	C(12)−O(12)	1.161(7)		

C(8)−Ru(1)−C(9)	87.6(2)	C(1)−Ru(1)−Ru(2)	134.1(1)	C(2)−Ru(1)−Ru(2)	92.8(1)	B(3)−Ru(1)−Ru(2)	57.4(1)
B(4)−Ru(1)−Ru(2)	76.3(2)	B(5)−Ru(1)−Ru(2)	124.2(1)	C(8)−Ru(1)−Ru(2)	98.8(1)	C(9)−Ru(1)−Ru(2)	101.6(2)
Ru(1)−B(3)−H(3)	114.4(1)	B(3)−H(3)−Ru(2)	110.1(2)	Ru(1)−B(4)−C(5)	111.5(3)	B(4)−C(5)−N(1)	110.6(4)
C(5)−N(1)−C(6)	108.0(4)	C(5)−N(1)−C(7)	108.3(3)	C(6)−N(1)−C(7)	106.9(4)	C(5)−N(1)−Ru(2)	112.0(2)
C(6)−N(1)−Ru(2)	112.8(2)	C(7)−N(1)−Ru(2)	108.7(3)	Ru(1)−C(8)−O(8)	177.0(4)	Ru(1)−C(9)−O(9)	176.7(4)
Ru(1)−Ru(2)−B(3)	50.2(1)	Ru(1)−Ru(2)−H(3)	74.6(2)	Ru(1)−Ru(2)−N(1)	92.6(1)	B(3)−Ru(2)−N(1)	82.2(1)
H(3)−Ru(2)−N(1)	87.0(2)	Ru(1)−Ru(2)−C(10)	84.4(2)	B(3)−Ru(2)−C(10)	133.8(2)	H(3)−Ru(2)−C(10)	159.0(3)
N(1)−Ru(2)−C(10)	93.0(2)	Ru(1)−Ru(2)−C(11)	85.5(2)	B(3)−Ru(2)−C(11)	95.7(2)	H(3)−Ru(2)−C(11)	91.5(2)
N(1)−Ru(2)−C(11)	177.8(2)	C(10)−Ru(2)−C(11)	87.9(2)	Ru(1)−Ru(2)−C(12)	176.3(2)	B(3)−Ru(2)−C(12)	128.8(2)
H(3)−Ru(2)−C(12)	104.0(2)	N(1)−Ru(2)−C(12)	90.7(2)	C(10)−Ru(2)−C(12)	97.0(2)	C(11)−Ru(2)−C(12)	91.2(2)
Ru(2)−C(10)−O(10)	177.0(5)	Ru(2)−C(11)−O(11)	176.6(5)	Ru(2)−C(12)−O(12)	172.1(3)		

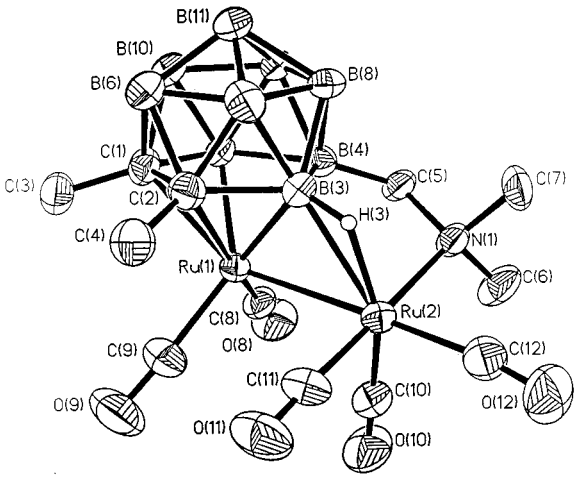

Figure 2. Molecular structure of [$Ru_2(\mu\text{-}\eta^5\text{-}7,8\text{-}Me_2\text{-}10\text{-}CH_2NMe_2\text{-}7,8\text{-}C_2B_9H_8)(CO)_5$] (**9**), showing the crystallographic labeling scheme. Except for H(3), hydrogen atoms have been omitted for clarity, and thermal ellipsoids are shown at 50% probability level.

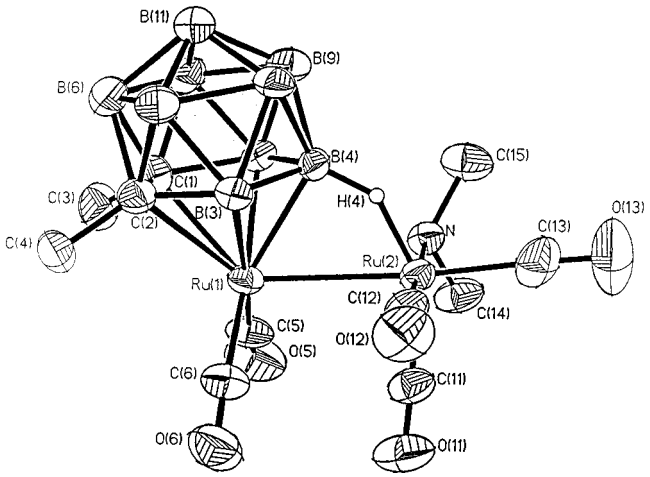

Figure 3. Molecular structure of [$Ru_2(CO)_5(NHMe_2)(\eta^5\text{-}7,8\text{-}Me_2\text{-}7,8\text{-}C_2B_9H_9)$] (**10**), showing the crystallographic labeling scheme. Except for H(4), hydrogen atoms have been omitted for clarity, and thermal ellipsoids are shown at 50% probability level.

of metal−metal bonds in **2** and a N−CH_2 bond in *N*,*N*,*N*′,*N*′-tetramethyldiaminomethane. This unexpected result prompted establishment of the structures of these molecules by single-crystal X-ray diffraction studies.

The molecular structure of **9** is shown in Figure 2, and selected parameters are listed in Table 5. The Ru(1)−Ru(2) bond [2.727(1) Å] is spanned by the *nido*-7,8-Me_2-10-CH_2NMe_2-7,8-$C_2B_9H_8$ group. The cage system is coordinated to Ru(1) by its open CCBBB face in the customary pentahapto manner while simultaneously forming exopolyhedral B(3)−H(3)⇀Ru(2) and B(4)−C(5)−N(1) bridges to Ru(2). The B−H⇀Ru unit involves B(3), the boron atom α to the carbons in the CC*B*BB ring, while the CH_2NMe_2 fragment is attached to B(4) which is in the β site with respect to the carbons in the CCB*B*B ring. Formally the CH_2NMe_2 cage substituent results from insertion of a C(H)NMe_2 group into a BH bond, although the actual pathway may well be different. There are five terminally bonded CO ligands, two coordinated to Ru(1) and three to Ru(2). Overall the molecule is electronically saturated for a dimetal compound with 34 valence electrons, with the cage contributing 8 and the CO groups 10 electrons.

The structure of **10** is shown in Figure 3, and the important bond distances and angles are listed in Table 6. The Ru(1)−Ru(2) bond distance [2.732(1) Å] is essentially the same as that in **9**. The *nido*-C_2B_9 cage ligates Ru(1) and forms an agostic bridge from the B(4)H(4) vertex to Ru(2). The latter carries an $NHMe_2$ ligand which lies in a cisoid position to the B_β−H⇀Ru(2) group. Two of the CO molecules are coordinated to Ru(1) and three to Ru(2). The molecule is electronically saturated with 34 valence electrons. At the present time the pathway for the formation of **9** and **10** from **2** and $Me_2NCH_2NMe_2$, which occurs under mild conditions, is unresolved, but interestingly it would seem that the donor reagent is fragmented into C(H)NMe_2 and $NHMe_2$ groups and that **2** must decompose to form $Ru_2(CO)_5(\eta^5\text{-}7,8\text{-}Me_2\text{-}7,8\text{-}C_2B_9H_9)$ fragments. The overall

Table 6. Selected Internuclear Distances (Å) and Angles (deg) for $[Ru_2(CO)_5(NHMe_2)(\eta^5\text{-}7,8\text{-}Me_2\text{-}7,8\text{-}C_2B_9H_9)]$ (10), with Estimated Standard Deviations in Parentheses

Ru(1)−C(1)	2.314(6)	Ru(1)−C(2)	2.316(6)	Ru(1)−B(3)	2.271(7)	Ru(1)−B(4)	2.203(7)
Ru(1)−B(5)	2.277(7)	Ru(1)−C(5)	1.844(7)	Ru(1)−C(6)	1.867(7)	Ru(1)−Ru(2)	2.732(1)
C(1)−C(2)	1.617(9)	C(1)−B(5)	1.731(10)	C(1)−B(6)	1.732(10)	C(1)−B(10)	1.720(10)
C(1)−C(3)	1.533(10)	C(2)−B(3)	1.712(10)	C(2)−B(6)	1.724(10)	C(2)−B(7)	1.706(10)
C(2)−C(4)	1.526(10)	B(3)−B(4)	1.800(11)	B(3)−B(7)	1.738(10)	B(3)−B(8)	1.780(10)
B(4)−H(4)	1.101	B(4)−B(5)	1.816(11)	B(4)−B(8)	1.768(10)	B(4)−B(9)	1.765(10)
B(4)−Ru(2)	2.419(7)	H(4)−Ru(2)	1.441	B(5)−B(9)	1.790(11)	B(5)−B(10)	1.774(10)
B(6)−B(7)	1.739(12)	B(6)−B(10)	1.720(12)	B(6)−B(11)	1.756(12)	B(7)−B(8)	1.762(11)
B(7)−B(11)	1.767(11)	B(8)−B(9)	1.786(11)	B(8)−B(11)	1.760(11)	B(9)−B(10)	1.782(12)
B(9)−B(11)	1.781(11)	B(10)−B(11)	1.759(12)	C(5)−O(5)	1.170(9)	C(6)−O(6)	1.158(9)
Ru(2)−C(11)	1.881(7)	Ru(2)−C(12)	1.873(7)	Ru(2)−C(13)	1.904(8)	Ru(2)−N	2.183(5)
C(11)−O(11)	1.164(9)	C(12)−O(12)	1.161(9)	C(13)−O(13)	1.159(11)	N−C(14)	1.477(8)
N−C(15)	1.496(8)						

C(5)−Ru(1)−C(6)	89.9(3)	C(5)−Ru(1)−Ru(2)	96.0(2)	C(6)−Ru(1)−Ru(2)	96.2(2)	Ru(1)−B(4)−H(4)	92.6(2)
Ru(1)−B(4)−Ru(2)	72.3(2)	B(4)−H(4)−Ru(2)	143.9(3)	Ru(1)−C(5)−O(5)	175.5(6)	Ru(1)−C(6)−O(6)	176.4(6)
Ru(1)−Ru(2)−B(4)	50.2(2)	Ru(1)−Ru(2)−H(4)	65.6(3)	Ru(1)−Ru(2)−C(11)	85.0(2)	B(4)−Ru(2)−C(11)	135.2(3)
H(4)−Ru(2)−C(11)	150.5(4)	Ru(1)−Ru(2)−C(12)	87.9(2)	B(4)−Ru(2)−C(12)	89.3(3)	H(4)−Ru(2)−C(12)	92.4(3)
C(11)−Ru(2)−C(12)	89.1(3)	Ru(1)−Ru(2)−C(13)	174.9(2)	B(4)−Ru(2)−C(13)	124.7(3)	H(4)−Ru(2)−C(13)	109.3(4)
C(11)−Ru(2)−C(13)	100.1(3)	C(12)−Ru(2)−C(13)	92.3(3)	Ru(1)−Ru(2)−N	91.0(1)	B(4)−Ru(2)−N	89.0(2)
H(4)−Ru(2)−N	86.0(3)	C(11)−Ru(2)−N	92.0(2)	C(12)−Ru(2)−N	178.4(2)	C(13)−Ru(2)−N	88.7(3)
Ru(2)−C(11)−O(11)	176.6(7)	Ru(2)−C(12)−O(12)	176.7(6)	Ru(2)−C(13)−O(13)	177.4(7)	Ru(2)−N−C(14)	115.8(4)
Ru(2)−N−C(15)	113.6(4)	C(14)−N−C(15)	109.8(5)				

low yield of **9** and **10** of ca. 25% is therefore not surprising.

The NMR data (Tables 2 and 3) for **9** and **10** are as expected from the crystal structure determinations. Both species show characteristic quartet resonances in the ^{1}H NMR spectra for the B−H⇀Ru bridges, that for **9** at δ −6.91 [J(BH) = 77 Hz] and that for **10** at δ −8.19 [J(BH) = 76 Hz]. Correspondingly, in the ^{11}B fully coupled NMR spectra there are doublets for these groups at δ 24.9 [J(HB) = 77] (**9**) and δ 26.6 [J(HB) = 76] (**10**). In the ^{1}H NMR spectrum of **9** the signals for the diastereotopic pair of BCH_2N protons are at δ 2.31 and 2.42. In both molecules the cage CMe groups are nonequivalent, and this is reflected in the ^{1}H NMR spectra with resonances for these groups at δ 2.22 and 2.30 (**9**) and δ 2.35 and 2.37 (**10**). However, in the ^{13}C-{^{1}H} NMR spectra, although the two resonances (**9**, δ 30.2 and 33.0; **10**, δ 31.8 and 31.9) anticipated for the C*Me* nuclei are observed, only one very broad peak is seen in the region for the *C*Me nuclei (**9**, δ 66.9; **10**, δ 65.1). This feature is not uncommon in ^{13}C{^{1}H} NMR spectra of metallacarboranes being evidently due to an overlap of signals whereas peaks in the ^{1}H NMR spectra are better resolved.

Treatment of **2** with pyridine in CH_2Cl_2 at room temperature gave a chromatographically separable mixture of the mono- and bis(pyridine)diruthenium complexes $[Ru_2(CO)_5(NC_5H_5)(\eta^5\text{-}7,8\text{-}Me_2\text{-}7,8\text{-}C_2B_9H_9)]$ (**11**) and $[Ru_2(CO)_4(NC_5H_5)_2(\eta^5\text{-}7,8\text{-}Me_2\text{-}7,8\text{-}C_2B_9H_9)]$ (**12**), data for which are given in Tables 1−3. The structure of **11** was determined by X-ray diffraction and is shown in Figure 4. Selected bond distances and angles are listed in Table 7. The molecule is structurally very similar to **10** but with a pyridine ligand replacing the $NHMe_2$ group. Again there is a B_β−H⇀Ru bridge involving B(4) the boron in the β site in the CCB*B*B ring. Not surprisingly the Ru(1)−Ru(2) distance in **11** [2.747(1) Å] is essentially the same as that in **10**. An X ray diffraction study on **12** was incomplete due to the poor quality of the crystal, but nevertheless it was apparent that it had a similar structure to **11** with the second pyridine molecule transoid to the metal−metal bond. In their ^{1}H NMR spectra both **11** and **12** show quartet resonances for the B−H⇀Ru groups at δ −7.82 [J(BH) = 80 Hz] and δ −5.28 [J(BH) = 67 Hz], respectively.

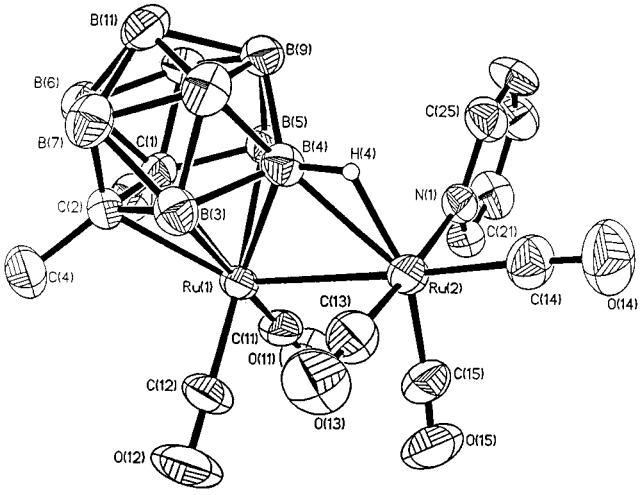

Figure 4. Molecular structure of $[Ru_2(CO)_5(NC_5H_5)(\eta^5\text{-}7,8\text{-}Me_2\text{-}7,8\text{-}C_2B_9H_9)]$ (**11**), showing the crystallographic labeling scheme. Except for H(4), hydrogen atoms have been omitted for clarity, and thermal ellipsoids are shown at 50% probability level.

Conclusions

There are several interesting aspects to the results described herein. Previous studies[1] showed that the reaction between *nido*-7,8-$C_2B_9H_{13}$ and $[Ru_3(CO)_{12}]$ yielded exclusively the monoruthenium complex **1a** whereas the present study reveals that the corresponding reaction with *nido*-7,8-Me_2-7,8-$C_2B_9H_{11}$ gives a mixture of **1b** and **2** in which the latter predominates. Interestingly, **1b** is not formed via the intermediacy of **2** since heating the latter at reflux temperatures in CH_2Cl_2 does not produce the former. The new triruthenium species **2** is likely to become a useful synthon providing a link between ruthenacarborane chemistry, where our present knowledge is very limited, and di- and trinuclear ruthenium carbonyl chemistry which has been extensively studied.[9] In this context it is noteworthy that several of the structures established are without precedent. The reactions of **2** with the various donor

Table 7. Selected Internuclear Distances (Å) and Angles (deg) for [$Ru_2(CO)_5(NC_5H_5)(\eta^5$-7,8-$Me_2$-7,8-$C_2B_9H_9$)] (11), with Estimated Standard Deviations in Parentheses

Ru(1)−C(1)	2.315(5)	Ru(1)−C(2)	2.315(5)	Ru(1)−B(3)	2.262(6)	Ru(1)−B(4)	2.191(6)
Ru(1)−B(5)	2.270(6)	Ru(1)−C(11)	1.868(6)	Ru(1)−C(12)	1.853(6)	Ru(1)−Ru(2)	2.747(1)
C(1)−C(2)	1.629(7)	C(1)−B(5)	1.719(7)	C(1)−B(6)	1.731(8)	C(1)−B(10)	1.716(8)
C(1)−C(3)	1.525(7)	C(2)−B(3)	1.722(8)	C(2)−B(6)	1.721(8)	C(2)−B(7)	1.727(8)
C(2)−C(4)	1.532(7)	B(3)−B(4)	1.782(9)	B(3)−B(7)	1.775(9)	B(3)−B(8)	1.782(9)
B(4)−H(4)	1.102	B(4)−B(5)	1.804(8)	B(4)−B(8)	1.776(9)	B(4)−B(9)	1.760(9)
B(4)−Ru(2)	2.416(6)	H(4)−Ru(2)	1.762	B(5)−B(9)	1.772(8)	B(5)−B(10)	1.772(8)
B(6)−B(7)	1.738(9)	B(6)−B(10)	1.749(9)	B(6)−B(11)	1.760(9)	B(7)−B(8)	1.757(9)
B(7)−B(11)	1.744(9)	B(8)−B(9)	1.778(9)	B(8)−B(11)	1.754(9)	B(9)−B(10)	1.769(9)
B(9)−B(11)	1.779(9)	B(10)−B(11)	1.777(9)	C(11)−O(11)	1.167(7)	C(12)−O(12)	1.157(8)
Ru(2)−C(13)	1.880(6)	Ru(2)−C(14)	1.917(6)	Ru(2)−C(15)	1.886(6)	Ru(2)−N(1)	2.168(4)
C(13)−O(13)	1.147(8)	C(14)−O(14)	1.152(7)	C(15)−O(15)	1.161(8)	N(1)−C(21)	1.328(7)
N(1)−C(25)	1.351(7)	C(21)−C(22)	1.375(8)	C(22)−C(23)	1.354(9)	C(23)−C(24	1.368(8)
C(24)−C(25)	1.359(8)						

C(11)−Ru(1)−C(12)	88.4(2)	C(1)−Ru(1)−Ru(2)	127.8(1)	C(2)−Ru(1)−Ru(2)	129.6(1)	B(3)−Ru(1)−Ru(2)	87.4(2)
B(4)−Ru(1)−Ru(2)	57.2(2)	B(5)−Ru(1)−Ru(2)	85.2(1)	C(11)−Ru(1)−Ru(2)	95.5(2)	C(12)−Ru(1)−Ru(2)	96.7(2)
Ru(1)−B(4)−H(4)	114.7(2)	B(4)−H(4)−Ru(2)	113.0(2)	Ru(1)−C(11)−O(11)	178.9(5)	Ru(1)−C(12)−O(12)	176.6(5)
Ru(1)−Ru(2)−B(4)	49.7(1)	Ru(1)−Ru(2)−H(4)	74.3(2)	Ru(1)−Ru(2)−C(13)	84.3(2)	B(4)−Ru(2)−C(13)	89.6(2)
H(4)−Ru(2)−C(13)	88.9(3)	Ru(1)−Ru(2)−C(14)	174.6(2)	B(4)−Ru(2)−C(14)	125.9(2)	H(4)−Ru(2)−C(14)	101.1(3)
C(13)−Ru(2)−C(14)	92.9(2)	Ru(1)−Ru(2)−C(15)	85.4(2)	B(4)−Ru(2)−C(15)	134.9(2)	H(4)−Ru(2)−C(15)	159.7(3)
C(13)−Ru(2)−C(15)	89.7(3)	C(14)−Ru(2)−C(15)	99.1(2)	Ru(1)−Ru(2)−N(1)	94.2(1)	B(4)−Ru(2)−N(1)	87.4(2)
H(4)−Ru(2)−N(1)	88.1(2)	C(13)−Ru(2)−N(1)	177.0(2)	C(14)−Ru(2)−N(1)	88.4(2)	C(15)−Ru(2)−N(1)	92.8(2)
Ru(2)−C(13)−O(13)	178.1(6)	Ru(2)−C(14)−O(14)	176.9(6)	Ru(2)−C(15)−O(15)	177.4(5)	Ru(2)−N(1)−C(21)	123.6(3)
Ru(2)−N(1)−C(25)	119.7(3)						

molecules afforded di- or triruthenium complexes depending on the donor reagent. Apparently nitrogen bases in particular favor formation of diruthenium complexes. However, further studies are merited to delineate which classes of donor molecule promote removal of a ruthenium fragment from the triruthenium precursor and which preserve the trinuclear framework.

Experimental Section

General Considerations. Solvents were distilled from appropriate drying agents under nitrogen prior to use. Petroleum ether refers to that fraction of boiling point 40−60 °C. All reactions were carried out under an atmosphere of dry nitrogen using Schlenk line techniques. Chromatography columns (ca. 15 cm in length and ca. 2 cm in diameter) were packed with silica gel (Aldrich, 70−230 mesh). TLC was performed on preparative UNIPLATES (silica gel G; Analtech). The compound *nido*-7,8-Me_2-7,8-$C_2B_9H_{11}$ was prepared from *closo*-1,2-Me_2-1,2-$C_2B_{10}H_{10}$ using a procedure similar to that for *nido*-7,8-$C_2B_9H_{13}$.[10] The NMR spectra were recorded at the following frequencies: ^{1}H 360.1, ^{13}C 90.6, ^{31}P 145.7, and ^{11}B 115.5 MHz.

Reaction of *nido*-7,8-Me_2-7,8-$C_2B_9H_{11}$ with [$Ru_3(CO)_{12}$]. The compounds [$Ru_3(CO)_{12}$] (0.34 g, 0.50 mmol) and *nido*-7,8-Me_2-7,8-$C_2B_9H_{11}$ (0.25 g, 1.50 mmol) were heated to reflux in CH_2Cl_2 (40 mL) for 24 h. The mixture was then cooled to room temperature and ca. 2 g of silica gel added. Solvent was removed *in vacuo* affording a reddish powder which was transferred to the top of a chromatography column. Elution with CH_2Cl_2−petroleum ether (1:4) gave an orange-red fraction. Removal of solvent *in vacuo* followed by crystallization from petroleum ether yielded orange-red microcrystals of [$Ru_3(CO)_8(\eta^5$-7,8-Me_2-7,8-$C_2B_9H_9$)] (**2**) (0.14 g). Further elution with CH_2Cl_2−petroleum ether (1:1) afforded a red band. Removal of solvent *in vacuo* from the eluate, followed by crystallization from CH_2Cl_2 layered with petroleum ether, gave crystals of [$Ru(CO)_3(\eta^5$-7,8-Me_2-7,8-$C_2B_9H_9$)] (**1b**) (0.05 g).

Reactions of [$Ru_3(CO)_8(\eta^5$-7,8-Me_2-7,8-$C_2B_9H_9$)] (2) with Phosphines. (i) A mixture of **2** (0.12 g, 0.17 mmol) and PPh_3 (0.045 g, 0.17 mmol) in THF (30 mL) was stirred at room temperature for ca. 15 h. Solvent was removed *in vacuo* and the dark red residue was dissolved in a minimum volume (ca. 5 mL) of CH_2Cl_2−petroleum ether (1:1) and chromatographed. Elution with CH_2Cl_2−petroleum ether (2:3) gave a dark yellow fraction, which after removal of solvent *in vacuo* yielded a red solid. The latter was crystallized from a CH_2Cl_2 solution on which a layer of petroleum ether was placed giving red crystals of [$Ru_3(\mu$-H)(μ-σ:η^5-7,8-Me_2-7,8-$C_2B_9H_8$)$(CO)_7(PPh_3)$] (**3**) (0.085 g).

(ii) Similarly, a mixture of **2** (0.34 g, 0.50 mmol) and PPh_3 (0.26 g, 1.0 mmol) was refluxed in THF (30 mL) for 2 h. After removal of solvent *in vacuo* the dark red residue dissolved in the minimum volume (ca. 5 mL) of CH_2Cl_2−petroleum ether (1:1) was chromatographed. Elution with CH_2Cl_2−petroleum ether (1:1) removed an orange-red fraction from which red crystals of [$Ru_3(\mu$-H)(μ-σ:η^5-7,8-Me_2-7,8-$C_2B_9H_8$)$(CO)_6(PPh_3)_2$] (**4**) (0.22 g) were obtained after crystallization from CH_2Cl_2−petroleum ether, as described above.

(iii) Compound **2** (0.13 g, 0.19 mmol) in CH_2Cl_2 (5 mL) was treated with an excess of PMe_2Ph (1 mL, 0.5 M THF solution, 0.50 mmol) and the solution stirred for 30 min. Use of TLC showed that no starting material remained. Petroleum ether (40 mL) was layered over the solution and the mixture placed in a freezer overnight. This procedure gave red crystals of [$Ru_3(\mu$-H)(μ-σ:η^5-7,8-Me_2-7,8-$C_2B_9H_8$)$(CO)_6(PMe_2Ph)_2$] (**5**) (0.13 g).

(iv) A mixture of **2** (0.17 g, 0.24 mmol) and PCy_3 (0.068 g, 0.24 mmol) was stirred at room temperature in CH_2Cl_2 (30 mL) for 3 h. Solvent was removed *in vacuo*, and the dark red residue was dissolved in a minimum volume (5 mL) of CH_2Cl_2−petroleum ether (1:1) and chromatographed. Elution with CH_2Cl_2−petroleum ether (2:3) removed a red band. Evaporation of solvent

(9) Deeming, A. J. In *Comprehensive Organometallic Chemistry II*; Abel, E. W., Stone, F. G. A., Wilkinson, G., Eds.; Pergamon Press; Oxford, U.K., 1995; Vol. 7 (Shriver, D. F., Bruce, M. I., Eds.), Chapter 12.

(10) Hlatky, G. G.; Crowther, D. J. *Inorg. Synth.*, in press. Young, D. A. T.; Wiersma, R. J.; Hawthorne, M. F. *J. Am. Chem. Soc.*, **1971**, *93*, 5687.

Table 8. Data for X-ray Crystal Structure Analyses[a]

	5	9	10	11
cryst dimens/mm	0.21 × 0.28 × 0.33	0.18 × 0.33 × 0.36	0.05 × 0.12 × 0.39	0.20 × 0.34 × 0.53
formula	$C_{26}H_{37}B_9O_6P_2Ru_3$	$C_{12}H_{22}B_9NO_5Ru_2$	$C_{11}H_{22}B_9NO_5Ru_2$	$C_{14}H_{20}B_9NO_5Ru_2$
M_r	908.0	559.7	547.7	581.7
cryst color, shape	orange irregular crystal	red parallelepiped	orange thin plate	red irregular crystal
cryst system	monoclinic	monoclinic	monoclinic	orthorhombic
space group (No.)	$P2_1/c$ (No. 14)	$P2_1/c$ (No. 14)	$P2_1/c$ (No. 14)	*Pbca* (No. 61)
a/Å	19.313(2)	15.511(2)	7.892(2)	11.842(1)
b/Å	15.448(2)	10.205(2)	14.303(2)	14.240(1)
c/Å	14.516(3)	14.818(2)	19.039(3)	26.405(1)
β/deg	95.67(1)	114.78(1)	96.91(2)	
V/Å^3	4323(1)	2129.6(6)	2233.4(6)	4452.7(5)
Z	4	4	4	8
d_{calcd}/g cm^{-3}	1.395	1.746	1.705	1.736
μ(Mo Kα)/cm^{-1}	11.19	14.14	14.09	13.56
F(000)/e	1792	1096	1072	2272
2θ range/deg	3−40	3−40	3−40	3−40
T/K	292	292	292	292
no. of reflns measd	4439	2233	2302	2604
no. of unique reflns	4016	1974	1995	2065
no. of obsd reflns	3216	1838	1596	1850
R_{int}	0.021	0.027	0.023	0.017
criterion for obsd *n* [$F_o \geq n\sigma(F_o)$]	$n = 4$	$n = 4$	$n = 4$	$n = 4$
weighting factor/*g*	0.0031	0.0001	0.0001	0.000 03
reflcn limits				
h	−18 to 18	−14 to 13	0 to 7	−2 to 11
k	0 to 14	0 to 9	0 to 13	−3 to 13
l	0 to 13	0 to 14	−18 to 18	−6 to 25
R (*R*′)[b]	0.0545 (0.0608)	0.0238 (0.0313)	0.0252 (0.0272)	0.0252 (0.0311)
final electron density diff features (max/min)/e Å^{-3}	1.57/−0.54	0.43/−0.28	0.36/−0.43	0.36/−0.38
S (goodness-of-fit)	1.50	1.72	1.17	1.71

[a] Data collected on an Enraf Nonius CAD4-F automated diffractometer operating in the ω−2θ scan mode; graphite-monochromated Mo Kα X-radiation, $\bar{\lambda} = 0.710\,73$. Refinement was by block full-matrix least-squares on *F* with a weighting scheme of the form $w^{-1} = [\sigma^2(F_o) + g|F_o|^2]$, where $\sigma^2(F_o)$ is the variance in F_o due to counting statistics. [b] $R = \sum||F_o| - |F_c||/\sum|F_o|$, $R' = \sum w^{1/2}||F_o| - |F_c||/\sum w^{1/2}|F_o|$.

in vacuo gave red microcrystals of [$Ru_3(\mu$-H)(μ-σ:η^5-7,8-Me_2-7,8-$C_2B_9H_8$)$(CO)_7(PCy_3)$] (**6**) (0.125 g).

(v) Compound **2** (0.22 g, 0.32 mmol) in CH_2Cl_2 (20 mL) was treated with an excess of PMe_3 (1 mL, 1.0 M THF solution, 1 mmol) and the mixture stirred for 10 min at room temperature. The volume of CH_2Cl_2 was reduced to ca. 2 mL, and CH_2Cl_2−petroleum ether (20 mL, 1:4) was added to give orange-red microcrystals of [$Ru_2(CO)_4$-$(PMe_3)_2(\eta^5$-7,8-Me_2-7,8-$C_2B_9H_9)$] (**7**) (0.13 g). Analytical pure **7** was obtained by crystallization from CH_2Cl_2 solutions layered with petroleum ether.

(vi) A mixture of **2** (0.21 g, 0.31 mmol) and dppm (0.12 g, 0.31 mmol) was stirred at room temperature in THF (30 mL) for 2 h. Solvent was removed *in vacuo*, and the residue extracted with CH_2Cl_2−petroleum ether (50 mL, 1:4). A white precipitate was filtered off, and the red filtrate was concentrated to ca. 20 mL. Red crystalline [$Ru_3(\mu$-dppm)$(CO)_6(\eta^5$-7,8-Me_2-7,8-$C_2B_9H_9)$] (**8**) (0.09 g) was obtained after storing the solution in a freezer overnight.

Reaction of [$Ru_3(CO)_8(\eta^5$-7,8-Me_2-7,8-$C_2B_9H_9)$] (2) with *N,N,N′,N′*-tetramethyldiaminomethane. A CH_2Cl_2 (30 mL) solution of **2** (0.20 g, 0.29 mmol) and $Me_2NCH_2NMe_2$ (40 μL, 0.29 mmol) was stirred at room temperature overnight. Solvent was removed *in vacuo* and the dark red residue dissolved in the minimum volume of CH_2Cl_2−petroleum ether (2:3) and chromatographed. Elution with CH_2Cl_2−petroleum ether (2:3) removed a broad orange fraction, which was concentrated and applied to a TLC plate. On eluting with CH_2Cl_2−petroleum ether (3:7), two yellow bands developed and were collected. After filtration and removal of solvent *in vacuo* the yellow solutions gave [$Ru_2(\mu$-η^5-7,8-Me_2-10-CH_2NMe_2-7,8-$C_2B_9H_8$)$(CO)_5$] (**9**) (7 mg) and [Ru_2-$(CO)_5(NHMe_2)(\eta^5$-7,8-Me_2-7,8-$C_2B_9H_9$)] (**10**) (35 mg), respectively, as orange-red solids. Analytically pure crystals of **9** and **10** were obtained by crystallization from CH_2Cl_2 solutions layered with petroleum ether.

Reaction of [$Ru_3(CO)_8(\eta^5$-7,8-Me_2-7,8-$C_2B_9H_9$)] (2) with Pyridine. Compound **2** (0.21 g, 0.30 mmol) and an excess of pyridine (72 μL, 0.89 mmol) in CH_2Cl_2 (30 mL) were stirred at room temperature for 2 h. Solvent was removed *in vacuo*, and the residue was dissolved in a minimum volume (ca. 5 mL) of CH_2Cl_2−petroleum ether (1:1) and chromatographed. The polarity of the eluting solvent CH_2Cl_2−petroleum ether was slowly increased from 1:4 to 1:1. Two orange colored bands developed. Elution of these fractions gave, after removal of solvent *in vacuo*, the complexes [$Ru_2(CO)_5$-$(NC_5H_5)(\eta^5$-7,8-Me_2-7,8-$C_2B_9H_9$)] (**11**) (14 mg) and [Ru_2-$(CO)_4(NC_5H_5)_2(\eta^5$-7,8-Me_2-7,8-$C_2B_9H_9$)] (**12**) (49 mg), respectively, both isolated as orange-red microcrystals. Analytically pure crystals of **11** and **12** were obtained by crystallization from CH_2Cl_2 solutions layered with petroleum ether.

Crystal Structure Determinations and Refinements. Crystal data and other experimental details for **5** and **9**−**11** are given in Table 8. Conoscopic examinations (Zeiss Photomicroscope II) of the crystals studied verified their biaxial nature and optical homogeneity, prior to their being mounted on glass fibers and transferred to the goniometer head on the diffractometer. Final lattice parameters were determined by least-squares refinement of 25 carefully centered high-angle reflections. No significant variations were observed in the periodic intensity measurements (2 h intervals) of compounds **5** and **9**. Hence, crystal stability and electronic hardware reliability were established. How-

ever, for complexes **10** and **11** decays of −0.10 and −0.06% h^{-1}, respectively, were corrected by employing the SDP program Decay,[11] which applied a linear decay correction to the data sets (maximum corrections, 1.05356 and 1.02582, respectively). The monitored check reflections of **5** and **9**−**11** were removed and the averaging of duplicate and equivalent data in each data set was carried out [R_{int} = 0.210 (**5**), 0.027 (**9**), 0.023 (**10**), and 0.016 (**11**)]. The remaining data in each data set were corrected for Lorentz, polarization, and X-ray absorption effects. For compounds **5**, **9**, and **11** empirical absorption corrections were applied[12] based on high-angle ψ scans (transmission factors: minimum, 0.9395, 0.8715, 0.8618; maximum, 0.9995, 0.9985, 0.9971, respectively). For compound **10** a numerical absorption correction[11] based on crystal face measurements was used (transmission factor: minimum, 0.8490; maximum, 0.9377). A zero moment test (NZ-test)[13] on the observed data sets indicated that all were centrosymmetric. Space group determinations were based on systematic absences, and the presence of any additional symmetry was ruled out by employing the MISSYM program.[14] Phase problems for the compounds studied were solved by utilizing the heavy-atom Patterson technique[15] which located all Ru atoms. Standard difference Fourier mapping yielded all other non-hydrogen atoms. Boron hydrogen atoms and bridging H atoms in **5** and **9**−**11** were located using the programs BHGEN[16] and XHYDEX,[5] respectively. The boron H atoms were fixed at a B−H distance of 1.10 Å (U_{iso} = 60 × 10^{-3} Å^2), and all carbon H atoms were idealized and held constant (C−H, 0.96 Å; U_{iso} = 80 × 10^{-3} Å^2). The models were refined using SHELXTL-PC programs,[15] and after application of secondary extinction corrections to each data set, anisotropic refinements of all non-hydrogen atoms yielded respectable residual indices. Final electron density maps revealed only random fluctuating backgrounds. Atomic scattering factors with related anomalous dispersion correction factors were obtained from the usual source.[17]

Acknowledgment. We thank the Robert A. Welch Foundation for support (Grants AA-1201 and -0668) and Dr. Paul Jelliss for helpful discussions.

Supporting Information Available: Complete tables of atomic coordinates, bond lengths and angles, anisotropic thermal parameters, and hydrogen atom parameters and ORTEP plots for **5** and **9**−**11** (34 pages). Ordering information is given on any current masthead page.

OM9603629

(11) Enraf-Nonius VAX Structure Determination Package, Delft, Holland, 1989.
(12) North, A. C. T.; Phillips, D. C.; Mathews, F. S. *Acta Crystallogr.* **1968**, *A24*, 351.
(13) Howells, E. R.; Phillips, D. C.; Rogers, D. *Acta Crystallogr.* **1950**, *3*, 210.
(14) Gabe, E. J.; LePage, Y.; Charland, J.-P.; Lee, F. L. *J. Appl. Crystallogr.* **1989**, *22*, 384.
(15) SHELXTL-PC, Siemens X-ray Instruments, Madison, WI, 1989.
(16) Sherwood, P. A program BHGEN for the calculation of idealized hydrogen atom positions for a *nido*-icosahedral carbaborane fragment, Bristol University, 1986.
(17) *International Tables for X-ray Crystallography*; Kynoch Press: Birmingham, U.K., 1974; Vol. 4.